# Magnetic properties of low-dimensional MAX₃

# (M=Cr, A=Ge, Si and X=S, Se, Te) systems

## M.S. Baranava✉, V.R. Stempitsky

Belarusian State University of Informatics and Radioelectronics, P. Brovki Str 6, 119, 220013, Minsk, Belarus

✉ baranova@bsuir.by

**Abstract.** The article presents the results of a magnetism study in quasi-two-dimensional MAX₃ (M=Cr, A=Ge, Si and X=S, Se, Te) systems. We calculated the microscopic magnetic parameters using quantum mechanical methods and showed that MAX₃ can have a high spin polarization. The easy magnetization axis lies normal to the layer plane. The main magnetic order of the $CrGeSe_3$, $CrGeTe_3$, $CrSiSe_3$, and $CrSiTe_3$ atomic systems is ferromagnetism. $CrGeS_3$ and $CrSiS_3$ exhibit antiferromagnetism. The low energy stability of the magnetic order is confirmed by the calculated values of the exchange interaction integral (J). We showed that the magnetic order realizes only at low temperatures. A study of the dependences of J and the magnetic anisotropy energy on the structural (distance between magnetic ions, distortion of the octahedral complex) and electronic properties (population and hybridization of atomic and molecular orbitals) has been performed. The dependences indicate three possible mechanisms of the exchange interaction. We have given ways of influencing a specific mechanism for managing exchange interaction.
**Keywords:** ab initio calculation, exchange energy, exchange integral, magnetic anisotropy, nanomagnetic, $CrSiS_3$, $CrGeTe_3$, $CrSiTe_3$

**Citation:** Baranava MS, Stempitsky VR. Magnetic properties of low-dimensional MAX₃ (M=Cr, A=Ge, Si and X=S, Se, Te) systems. *Materials Physics and Mechanics*. 2022;49(1): 73-84. DOI: 10.18149/MPM.4912022_5.

## 1. Introduction
Low-dimensional magnetism is a quantum cooperative phenomenon. It belongs to the promising area of research in condensed matter physics. The objects under study are atomic systems in which the magnetic interaction is limited in one or more spatial directions. The Mermin-Wagner-Hohenberg (1966) theorem [1] states that thermal fluctuations destroy the long-range magnetic order at any finite temperature in low-dimensional isotropic magnetic systems. However, confirmation of the possibility of low-dimensional magnetism in monolayer samples was presented earlier (1944) in the theoretical work [2]. The arising contradictions are explained by different representations of spin magnetic moments in the Ising model [3], which was used in the work by Onsager, and the Heisenberg model [4], which was used for the proof of the Mermin-Wagner-Hohenberg theorem [1].

Limiting the dimensionality of magnetic systems can lead to strong magnetic anisotropy [5]. In this case, the vector of the magnetic moment of an atom has an orientation along only one crystallographic direction. The total spin of atoms has only one spatial coordinate. The Heisenberg model is not suitable for describing such materials. Therefore, the Mermin-Wagner-Hohenberg theorem, which is valid only for the isotropic Heisenberg model, cannot be applied to low-dimensional magnets. Such atomic structures are usually represented within the framework of the Ising model, which provides for only one degree of freedom of the magnetic moment of an atom [6]. These materials belong to the class of Ising magnets [7].

In 2016, a new stage began in the physics of low-dimensional magnetism due to the development of mechanical and chemical exfoliation of thin films from van der Waals structures [8]. These structures have strong chemical bonds in the layer plane and weak interplanar bonds. Such structure leads to a strong magnetic uniaxial anisotropy in the monolayer which is necessary for observing low-dimensional Ising-type magnetism.

Low-dimensional ferromagnetic order (FM) was implemented in unstable structures [8-13]. Also, the magnetic order was obtained in van der Waals systems for bulk modifications [14-29] which structures consist of several layers [30-34]. A stable low-dimensional magnetic order at a high Curie temperature (room temperature) has not yet been realized. Ternary $MAX_3$ (M=Cr, A=Ge, Si and X=S, Se, Te) compounds are van der Waals structures. The bulk phase consists of three monolayers located through the van der Waals gap with ABC stacking (Fig. 1).
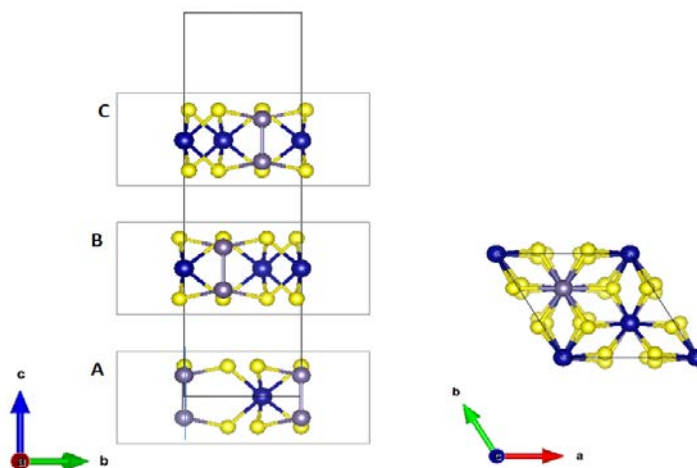


**Fig. 1.** Structure of transition metal chalcogenide $MAX_3$

The energy of magnetocrystalline anisotropy and the energy of exchange interaction make the dominant contributions to the magnetic energy of an atomic system for low-dimensional magnets as was shown by using quantum mechanical calculations. Spin-orbit interaction and exchange interaction are the sources of these contributions. These phenomena have a strict dependence on the composition, structure, and electronic properties of materials.

For practical applications of low-dimensional magnetic materials, research efforts should be directed to such important issues as increasing $T_c$ for the operation of spintronic devices at room temperatures and above, searching for two-dimensional materials with magnetic anisotropy in the sample plane to reduce the switching current and increasing the residual magnetic induction. Such materials with magnetic anisotropy energy more than the thermal activation energy $k_B T$, having reduced thermal noise, expand the element base.

The article presents the study of the relationship between the composition, structure, magnetic and electronic properties in the framework of quantum mechanical calculation of microscopic magnetic parameters. Theoretical substantiation of the $MAX_3$ properties allows

finding ways to enhance the magnetic energy and furnish insight into the nature of low-dimensional magnetism.

**2. Methods**

The study of $MAX_3$ magnetic parameters was carried out in several stages. In the first stage, the quantum mechanical calculation was carried out with spin polarization preliminary ionic relaxation in the VASP software package [35]. Static self-consistent calculations were performed for the ground state structural parameters. Calculations of the ground quantum state band structures were carried out for the Γ-K-M-Γ contour in the Brillouin zone. In the second stage, the microscopic magnetic parameters were calculated. The exchange interaction integral was calculated using the Heisenberg model [4].

Computational cells consisting of 2×2×1 elementary cells were created to take into account the exchange interaction between the central Cr ion and the first ($J_1$), second ($J_2$), and third nearest magnetic ion. Four magnetic configurations were set for each cell, three corresponding to the antiferromagnetic state and one to the ferromagnetic state (Fig. 2).
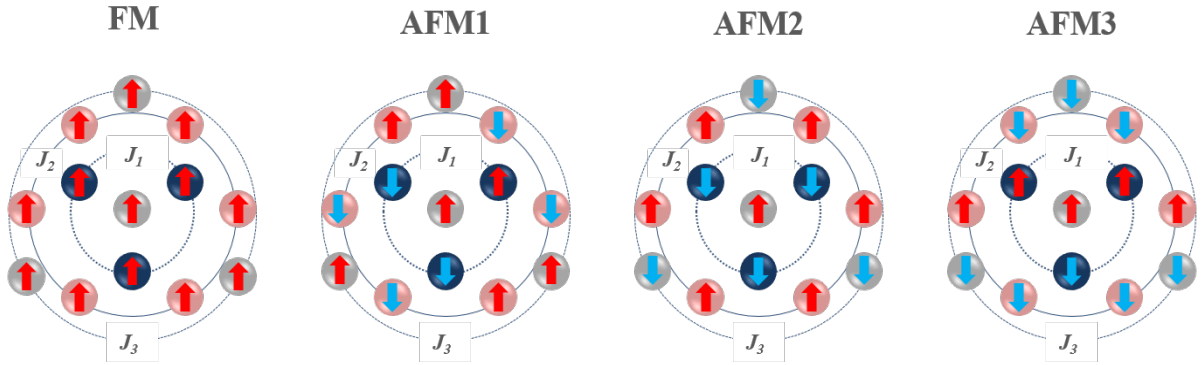


**Fig. 2.** Magnetic configurations of the chromium sublattice

The equations of the total energy of the system for four magnetic configurations are:

$$E_{AFM1} = E_0 + \frac{1}{2}S^2(-J_1 - J_2 + J_3), \qquad (1)$$

$$E_{AFM3} = E_0 + \frac{1}{2}S^2(J_1 - J_2 - J_3), \qquad (2)$$

$$E_{AFM2} = E_0 + \frac{1}{2}S^2(-3J_1 + 3J_2 - J_3), \qquad (3)$$

$$E_{FM} = E_0 + \frac{1}{2}S^2(3J_1 + 3J_2 + J_3). \qquad (4)$$

The computational cells of quasi-two-dimensional atomic structures were optimized for all considered magnetic configurations, which are presented in Fig. 2. The final structural parameters correspond to the ground magnetic state.

The Curie temperature ($T_c$) was calculated using the equation:

$$T_C = 2zJS(S + 1)/3k_B, \qquad (5)$$

where $z$ is the number of the nearest neighbors, $S$ is the spin of the magnetic ion, $k$ is Boltzmann constant.

Spin polarization was calculated by the equation:

$$P = (n_\uparrow - n_\downarrow)/(n_\uparrow + n_\downarrow), \qquad (6)$$

where $n_\uparrow$ is the density of states of electrons with spin up, $n_\downarrow$ is the density of states of electrons with spin down.

The deviation of the angles of the octahedral complex from the ideal value was calculated by the equation [36]:

$$\varsigma^2 = \sum_{i=1}^{n}[(\theta_i - 90)^2/6], \qquad (7)$$

where $\theta_i$ is the bond angle in the octahedral complex.

In the third stage, the dependence of microscopic magnetic parameters on structural and electronic properties was analyzed.

## 3. Results and Discussion

**Quantum mechanical simulation.** An analysis of the magnetization distribution showed a local magnetic moment on Cr atoms, which ranges from 2.94 to 3.44 $\mu_B$. This indicates the presence of three electrons with uncompensated spins. Therefore, the chromium atom in $MAX_3$ compounds is an ion with a charge of +3e ($Cr^{3+}$). According to the calculations, 90-95% of the total magnetic moment is localized on the d-orbitals of $Cr^{3+}$. It makes it possible to use magnetic models based on the principles of localized electronic states, such as the Ising and Heisenberg models [3,4], as well as to interpret the results in terms of the crystal field theory.

The main magnetic order of the studied compounds is FM, except for those compounds where S acts as a chalcogen. In this case, the main magnetic order is AFM. Deviation of the local magnetic moment from an integer value upwards is observed in compounds with FM, and downwards in compounds with AFM. It indicates the possible hybridization of $Cr^{3+}$ d-electrons with surrounding ions. A study of this issue is given below.

Electronic properties calculations of the $MAX_3$ two-dimensional configurations for the main magnetic states show that all compounds are indirect-gap semiconductors. Figure 3 presents the band structure of $CrSiSe_3$ as an example. The top of the valence band is at the $\Gamma$-point. The bottom of the conduction band is located between points M and $\Gamma$.
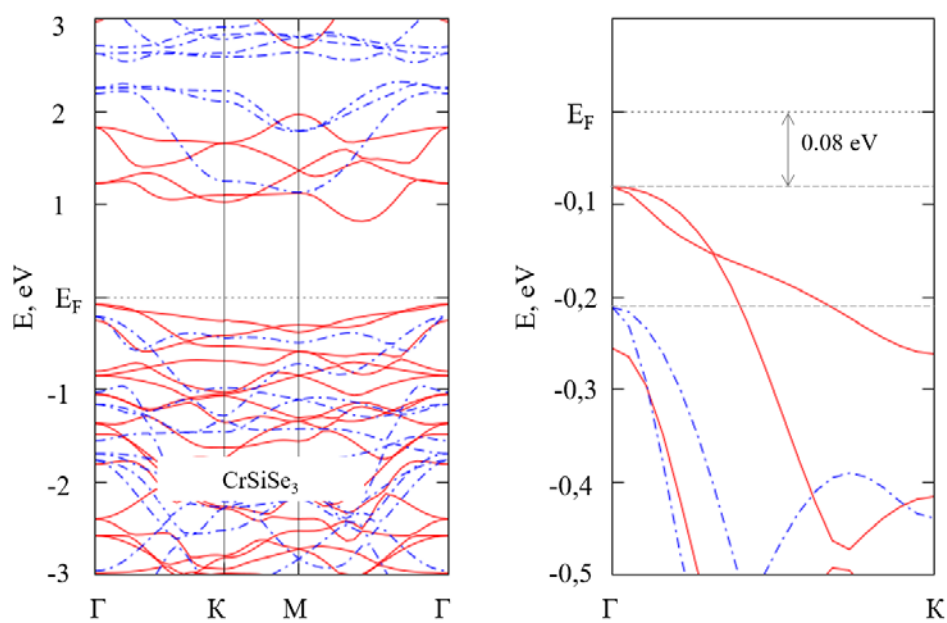


**Fig. 3.** $CrSiSe_3$ band structure
(Red solid bands correspond to the energy states of electrons with spin up, and blue dash bands correspond to the energy states of electrons with spin down)

The bottom of the conduction band is formed due to the d-orbitals of Cr. The p-orbitals of chalcogens make the main contribution to the formation of the top of the valence band in all cases, except for AFM atomic systems with X=S. In this case, the top of the valence band is formed by the d-orbitals of Cr, the p-orbitals of chalcogens, and the p-orbitals of Ge and Si ions. In the $CrGeS_3$ compound, p-orbitals of Ge prevail in the formation of the top of the valence band. The band gaps for the two spin subsystems differ by factors of 1.51 and 1.60 ($E_g^{up}$ /$E_g^{dw}$) in $CrSiSe_3$ and $CrSiTe_3$, respectively. This makes it possible to generate the

motion of spin-polarized charge carriers with a large polarization coefficient. The energy gap between the top of the valence band and $E_f$ ranges from 0.08 eV to 0.18 eV. These values are 0.08 eV and 0.11 eV for $CrSiSe_3$ and $CrSiTe_3$, respectively.

With an increase in temperature or the application of an external electric field, it is possible to change the band structure from a semiconductor type of conductivity to a metal one. The conductivity, similar to a semimetallic, can be obtained for $CrSiSe_3$ and $CrSiTe_3$ using an external action.

**Calculation of microscopic magnetic parameters in MAX$_3$.** The exchange interaction integral was calculated based on the results of the local magnetic moments simulation and using the Heisenberg Hamiltonian. Spin in equations (1-4) is taken as 3/2 because the magnetic moment has a strong localization on $Cr^{3+}$. The equations for calculating the exchange interaction integral are determined through the difference in energies of various magnetic configurations:

$$J_1 = (-E_{AFM2} + E_{AFM3} + E_{FM} - E_{AFM1}), \tag{8}$$
$$J_2 = \frac{(E_{AFM2} - E_{AFM3})}{288} + J_1, \tag{9}$$
$$J_3 = \frac{(E_{AFM3} - E_{AFM1})}{216} + J_1. \tag{10}$$

The exchange interaction integrals calculated are given in Table 1.

Table 1. Microscopic magnetic parameters

| MAX$_3$ | $J_1$, meV | $J_2$, meV | $J_3$, meV | $E_{MAE}$, meV | $T_c$, K | $P$ | $d_{M-M}$, Å | $\alpha_{Cr-X-Cr}$, deg | $\varsigma^2$, deg$^2$ |
|---------|-----------|-----------|-----------|----------------|----------|------|--------------|-------------------------|------------------------|
| CrGeS$_3$ | -0.06 | 0.04 | 0.09 | – | – | – | 3.47 | 91.31 | 51.52 |
| CrGeSe$_3$ | 0.68 | -0.18 | 0.0005 | -0.55 | 59.22 | 0.69 | 3.64 | 90.87 | 72.61 |
| CrGeTe$_3$ | 2.07 | 0.04 | 0.50 | -0.27 | 180.50 | 0.38 | 3.98 | 92.14 | 47.98 |
| CrSiS$_3$ | -1.53 | 0.17 | 0.01 | – | – | – | 3.40 | 88.68 | 39.18 |
| CrSiSe$_3$ | 1.74 | -0.13 | 0.07 | -0.92 | 151.68 | 0.98 | 3.99 | 91.82 | 37.00 |
| CrSiTe$_3$ | 1.48 | -0.03 | -0.16 | -0.28 | 129.01 | 0.73 | 3.98 | 89.71 | 32.19 |

**Dependence of microscopic magnetic parameters on electronic properties.** In the MAX$_3$ atomic structures, the $Cr^{3+}$ ion is surrounded by six chalcogen ligands (Fig. 4a). This allows analyzing the electronic properties within the framework of the theory developed for octahedral complexes. The crystal field of the ligands causes the $d$-orbitals to split into three-fold degenerate states ($t_{2g}$), which consist of $d_{xy}$, $d_{zx}$ and $d_{yz}$, and two-fold degenerate states ($e_g$), which consist of $d_{z2}$ and $d_{x2-y2}$.

Before calculating the partial density of electronic states (DOS), the vectors of the computational cells were rotated. Accordingly, the bonds between the vertices of the octahedron (chalcogen ions) and the $Cr^{3+}$ located in the center were parallel to the axes of the Cartesian coordinate system (Fig. 4a). Otherwise, the calculation results will show a non-standard linear combination of atomic orbitals and "mixing" of partial DOS. This impedes analyzing the results. The partial DOS for $Cr^{3+}$ $d$-electrons with rotated computational cells shows the classical splitting of energy levels into $t_{2g}$ and $e_g$ states (Fig. 4b).

Figure 5 shows the obtained partial DOS for octahedral complexes consisting of $Cr^{3+}$ and ligands in the corresponding MAX$_3$ compounds.
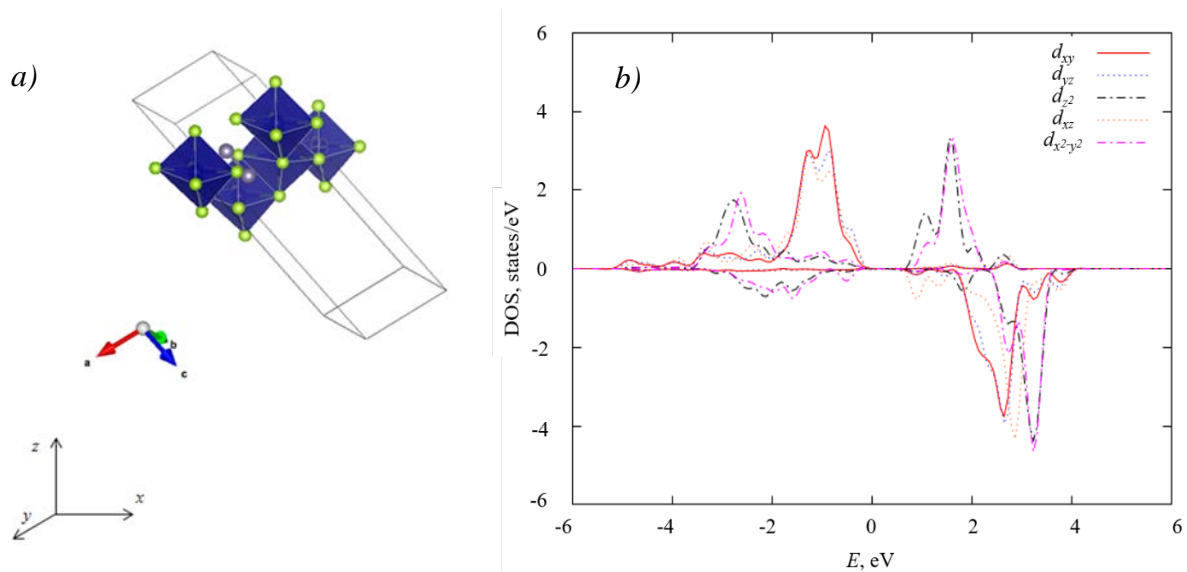
**Fig. 4.** Rotated computational cell (*a*); partial DOS of d-electrons (*b*)

A common feature of the obtained partial DOS is the existence of localized $t_{2g}$ states that are located below the Fermi level for electrons with spins up, i.e., correspond to filled states, and also above the Fermi level, i.e., correspond to unoccupied states. Unoccupied $e_g$ orbitals have energy higher than $t_{2g}$. The energy difference between these orbitals is determined by electrostatic splitting and is responsible for the formation of the high-spin state. In all atomic systems, this parameter does not change. The presence of filled $e_g$ levels is explained by the hybridization of the corresponding atomic states of $Cr^{3+}$ and surrounding ions, which leads to the formation of a common molecular orbital σ with decreasing energy. The energy split between $t_{2g}$ and σ characterizes the degree of hybridization. In compounds with X=Se, the energy difference between filled molecular orbitals and $t_{2g}$ orbitals is higher than in atomic systems with Te, which indicates greater hybridization, since more overlap leads to an energetically favorable state.

Bader analysis [37] presents that 5.8 electrons are located on the $t_{2g}$ orbitals of $Cr^{3+}$ ions. This value is unchangeable for all atomic systems. The molecular orbital σ contains 8.40 and 8.50 spin-up electrons, as well as 8.10 and 8.15 spin-down electrons in the $CrSiSe_3$ and $CrGeSe_3$ atomic systems, respectively. For $CrSiTe_3$ and $CrGeTe_3$, the corresponding values are 7.70 and 7.65 spin-up electrons and 7.10 and 7.15 spin-down electrons. Changes in the population of molecular orbitals are observed only when the chalcogen changes, and do not depend on other components of the atomic system. The increase in this value occurs due to the electronegativity of the chalcogen *p*-orbital (2.10 for Te, 2.55 for Se). Therefore, the degree of hybridization is affected by the *p*-orbitals of the chalcogen.

We can conclude that Si and Ge do not have a direct effect on the corresponding dependencies between electronic properties and magnetic parameters, because the σ population depends only on the chalcogen, and $t_{2g}$ in the structures under study is determined by the crystal symmetry. Thus, it suffices to analyze the influence of ligands on $J$ to formulate the dependencies of the magnetic parameters on the electronic properties.

The electronic configurations of ligand atoms have the form: Te [Kr] $3d^{10}5s^25p^4$, Se [Ar] $3d^{10}4s^24p^4$, S [Ne] $3s^23p^4$. The difference between the electronic configurations is the main quantum number (n) of the outer valence shell, while the filling of the sublevels is similar. The value of $J_3$ increases with increasing n (Table 1), which characterizes the exchange interaction with the third neighboring magnetic ion. Therefore, the diffuseness of the valence shell affects the longest-range exchange interaction, i.e. $J_3$. For example, the outer electron shell Te has a higher n and is more diffuse. Thereby $CrGeTe_3$ and $CrSiTe_3$ have the

highest modulus $J_3$. Also, the diffuseness of the Te valence shell suggests the weakest hybridization in atomic systems with this element, and consequently the smaller exchange interaction $J_1$. The energy difference between the occupied $e_g$ and $t_{2g}$ states is larger for $CrGeSe_3$ than for $CrGeTe_3$ according to the partial DOS (Fig. 3). The formation of a molecular orbital in $CrGeSe_3$ is energetically more favorable, and hybridization should be stronger. However, the calculation results for $J_1$ confirmed the above conclusion for compounds with A=Si but did not demonstrate this dependence for compounds with A=Ge. This is explained by the strong influence of structural parameters on magnetic properties.
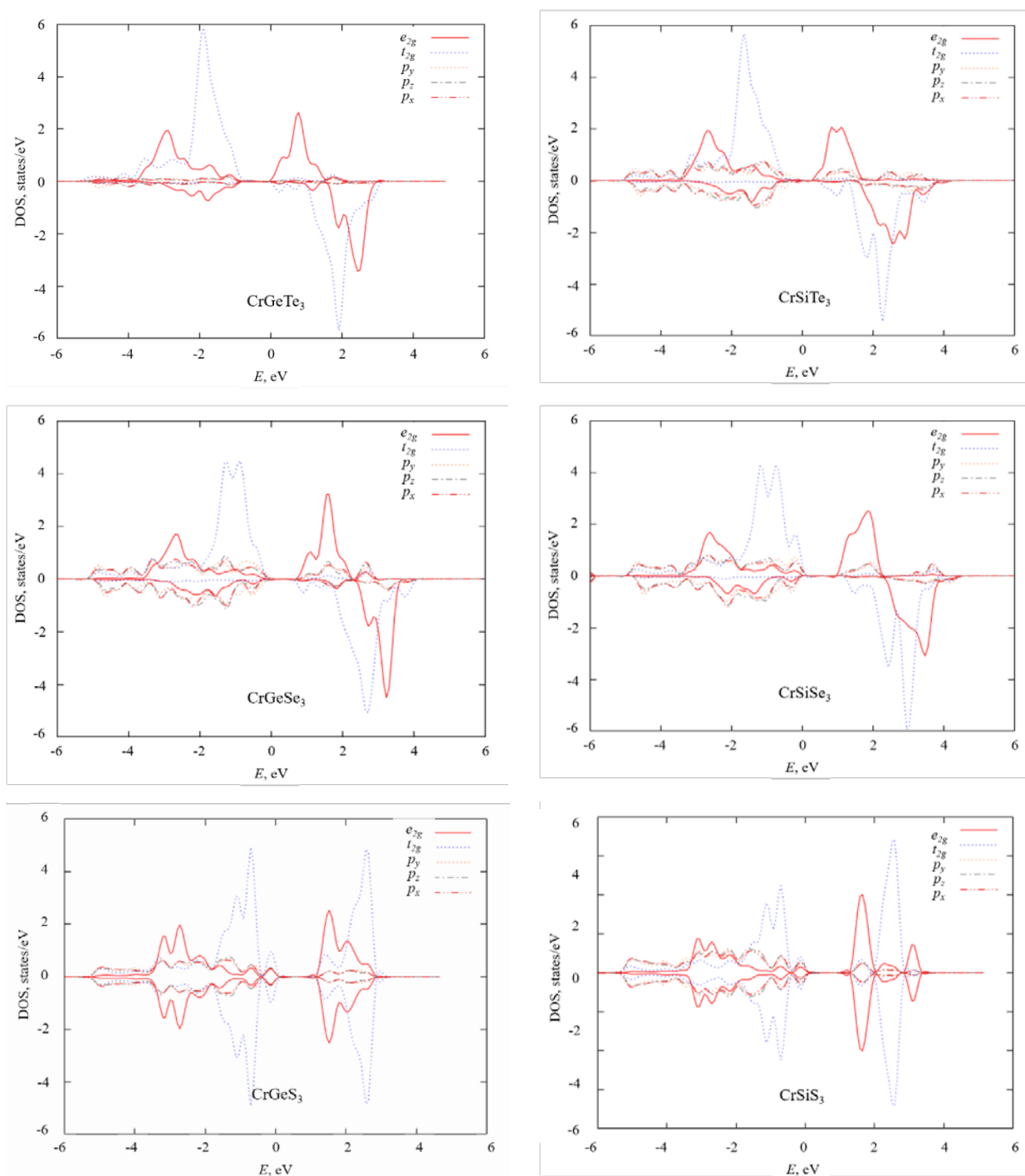


**Fig. 5.** Partial DOS of $MAX_3$ two-dimensional atomic systems

**Dependence of microscopic magnetic parameters on the structural properties.** Atomic systems with Ge have a larger value of $\varsigma^2$ (Table 1) compared to atomic systems containing Si. Since $E_{MAE}$ (Table 1) depends on the crystal field [38], the symmetry lowering should cause modulation of this microscopic parameter. In $CrSiSe_3$ and $CrGeSe_3$, the $\varsigma^2$ values are 37.00 and 72.61 $deg^2$, respectively, which leads to a decrease in $E_{MAE}$ from 0.92 meV to 0.55 meV. In $CrSiTe_3$ and $CrGeTe_3$, the difference in $\varsigma^2$ values is not so significant and equals 32.19 and 47.98 $deg^2$, respectively. It leads to insignificant changes in the $E_{MAE}$ values (0.28 and 0.27 meV, respectively). This behavior is explained by the different diffuseness and the degree of deformation of $p$-orbitals of chalcogens. Therefore, lattice distortion affects the $E_{MAE}$ to a lesser extent in compounds where the chalcogens have a larger $n$ value. Thus, $E_{MAE}$ has a significant dependence on Si and Ge, as well as on chalcogen.

$CrGeTe_3$, $CrSiSe_3$, $CrSiTe_3$ have a distance between the two nearest $Cr^{3+}$ ($d_{M-M}$) in the range from 3.98 to 3.99 Å. Moreover, these compounds possess FM. In $CrGeSe_3$, this parameter is 3.64 Å, while the exchange interaction between the two nearest $Cr^{3+}$ indicates FM several times weaker than in $CrGeTe_3$, $CrSiSe_3$, and $CrSiTe_3$. In $CrGeS_3$ and $CrSiS_3$ the $d_{M-M}$ are 3.47 and 3.40 Å, and the exchange interaction is AFM. A decrease in the distance between the nearest $Cr^{3+}$ leads to a weakening of the FM and an increase in the AFM. This dependence indicates the direct exchange interaction responsible for the AFM. The difference in $J_1$ for $CrSiS_3$ and $CrGeS_3$ is then explained by the strong dependence of the direct exchange interaction on the symmetry breaking of the crystal. Direct exchange interaction enhances AFM, but FM dominates in the compounds where $d_{M-M}$ has a large value. Thus, the dominant mechanism of the exchange interaction between $Cr^{3+}$ in $CrGeSe_3$, $CrGeTe_3$, $CrSiSe_3$, and $CrSiTe_3$ is superexchange through chalcogen atoms. The above conclusion confirms the Goodenough-Kanamori-Anderson rule [39], which states that superexchange interaction is possible between half-filled $Cr^{3+}$ $d$-orbitals and filled ligand orbitals at a value of $\alpha_{Cr-X-Cr}$ close to 90 deg.

**Exchange interaction mechanism.** Figure 4 shows two octahedral complexes with central Cr atoms connected through common vertices. Chalcogens are located in the vertices. The spatial arrangement of Cr in the environment of chalcogens leads to the emergence of six hybrid atomic orbitals of the $sp^3d^2$ type in Cr, which consist of $d_{z2}$, $d_{x2-y2}$, $s$, $p_x$, $p_y$, $p_z$ according to Pauling's hybridization theory. These orbitals correspond to bonding states. The other three orbitals $d_{xz}$, $d_{yz}$ and $d_{xy}$ keep atomic-like ($t_{2g}$ according to the crystal field theory). They are filled with electrons, which form the intrinsic magnetic moment of the transition metal. The hybrid atomic orbitals are directed from the central atom towards the vertices of the octahedral complex, where they bond with the $p$-orbitals of the chalcogen and form the bonding molecular orbital $\sigma$.

Exchange interaction is possible to implement by three mechanisms. The first mechanism occurs between $d$-orbitals of the same symmetry ($t_{2g}$) of two $Cr^{3+}$. This is a direct kinetic exchange ($J_{kin}$, Fig. 6). The interaction angle is 180° or close to it, and the exchange occurs between partially filled orbitals. In this case, according to the Goodenough-Kanamori-Anderson rules, AFM can be formed. The evidence for the implementation of this mechanism into $MAX_3$ is based on the following: the distance decrease between two nearest $Cr^{3+}$ weakens FM and increases AFM. Besides the larger $\varsigma^2$ is in compounds with AFM ($CrSiS_3$ and $CrGeS_3$), the smaller $J_1$.

The second mechanism is carried out due to electron hopping (tunneling) between the molecular orbital $\sigma$ of the first $Cr^{3+}$ and $t_{2g}$ atomic orbitals of the second $Cr^{3+}$ ($J_{te}$, Fig. 6). The proof for the implementation of this mechanism rests on the results listed below. Firstly, the hybridization of $sp^3d^2$ orbitals with p-orbitals of the chalcogen was observed in all studied atomic systems (i.e., $\sigma$ orbital) in accordance with the partial DOS presented in Fig. 3. Secondly, the exchange occurs between an empty electron shell and a partially filled one, the

valence angle of exchange interaction path having a value close to 90° (from 88.68° to 92.14°). According to the Goodenough-Kanamori-Anderson rules, such an exchange interaction is a superexchange interaction that forms FM. Thirdly, the FM increases with increasing $d_{M-M}$, which indicates a weakening possible direct exchange interaction, which is the AFM.

The third mechanism is AFM. It occurs between $t_{2g}$ orbitals of different symmetry on two $Cr^{3+}$ through hybridization with $p$-orbitals of the chalcogen ($J_{tt}$, Fig. 6). This exchange is insignificant and is determined by a small deviation of the local magnetic moment on the $t_{2g}$ orbitals. The total exchange interaction integral consists of contributions given by each exchange interaction mechanism:

$$J = J_{tt} + J_{kin} + J_{te}. \tag{11}$$

The first and second terms of the equation are responsible for the AFM. The third term has a negative sign and reflects the contribution of the FM. Thus, to form a stable high-temperature FM, it is necessary to increase $J_{te}$ using strategies aimed at enhancing hybridization and/or decreasing $J_{tt}$ and $J_{kin}$ using strategies that affect structural properties.
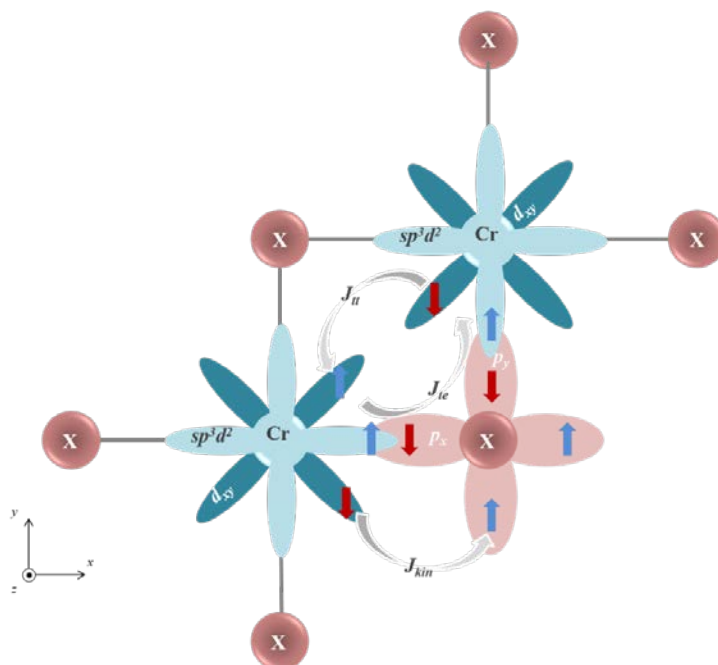


**Fig. 6.** Mechanisms of exchange interaction

**Influence of the Hubbard coefficient on the simulated magnetic order.** The hybridization of electron orbitals is highly dependent on the Hubbard coefficient ($U$) in quantum mechanical calculations. Since hybridization is the key phenomenon that determines the dominant exchange interaction mechanism in $MAX_3$, then $U$ can have a strong influence on the main magnetic order and the quantitative value of J. We performed quantum mechanical calculations of $J_1$ for various $U$ (Table 2).

AFM weakens as $U$ increases from 0 to 3 eV, in $CrSiS_3$. The weak AFM in $CrGeS_3$ transforms into an unstable FM. FM is enhanced in other atomic systems. The choice of $U$ remains an important criterion for characterizing the exchange interaction. The differences between the results of similar theoretical works mainly lie in different choices of this parameter.

Table 2. Exchange interaction integral for different values of $U$, meV

| MAX$_3$ | $J_1$ ($U$=0 eV) | $J_1$ ($U$=1 eV) | $J_1$ ($U$=3 eV) |
|---------|------------------|------------------|------------------|
| CrGeS$_3$ | 0.72 | 0.06 | -0.39 |
| CrGeSe$_3$ | -0.18 | -0.68 | -1.04 |
| CrGeTe$_3$ | -1.73 | -2.07 | -2.35 |
| CrSiS$_3$ | 2.47 | 1.53 | 0.85 |
| CrSiSe$_3$ | -1.59 | -1.74 | -1.88 |
| CrSiTe$_3$ | -1.26 | -1.48 | -1.61 |

## 4. Conclusions

The main magnetic order of CrGeSe$_3$, CrGeTe$_3$, CrSiSe$_3$, and CrSiTe$_3$ atomic systems is FM. CrGeS$_3$ and CrSiS$_3$ exhibit AFM. 90-95% of the total magnetic moment is localized on the $d$-orbitals of Cr$^{3+}$ and ranges from 2.94 to 3.44 $\mu_B$. A slight deviation from the integer value indicates the hybridization of the Cr$^{3+}$ $d$-electrons with the surrounding ions.

Increasing the principal quantum number of the outer electron shell of the chalcogen leads to weakening the hybridization of the atomic orbitals of Cr$^{3+}$ and surrounding ions, with the formation of a common molecular orbital σ, as well as increasing $J_3$. Si and Ge do not have a direct influence on the relationships between electronic properties and magnetic parameters. An increase in $d_{M-M}$ leads to FM, as well as an increase in $\varsigma^2$ in AFM compounds (CrSiS$_3$ and CrGeS$_3$) leads to a decrease in the value of $J_1$.

The found dependencies indicate three competing mechanisms of exchange interaction. FM is formed due to the mechanism of superexchange interaction. AFM exchange interaction is carried out by kinetic direct exchange and superexchange interaction.

It has been established that the axis of easy magnetization lies normal to the plane of quasi-two-dimensional layers, i.e., along the [001] crystallographic direction. This provides an increase in the energy efficiency of spintronic devices. $T_c$ for the studied compounds lying in the range from 59.22 to 129.01 K. To form a stable high-temperature FM, the exchange interaction by the superexchange FM mechanism should be increased using strategies aimed at enhancing hybridization (external electric field, deformation), and/or reducing AFM direct exchange interaction through the use strategies that affect structural properties (deformation). Another way is to increase the $E_{MAE}$ by varying the composition.

## References

1. Mermin ND, Wagner H. Absence of ferromagnetism or antiferromagnetism in one-or two-dimensional isotropic Heisenberg models. *Physical Review Letters*. 1966;17(22): 1133.
2. Onsager L. Crystal statistics. I. A two-dimensional model with an order-disorder transition. *Physical Review*. 1944;65(3-4): 117.
3. Singh SP. The Ising model: Brief introduction and its application. In: *Solid State Physics-Metastable, Spintronics Materials and Mechanics of Deformable Bodies-Recent Progress.* IntechOpen; 2020.
4. Nowak U. Classical spin models. In: *Fundamentals of micromagnetism and discrete computational models.* Wiley; 2007. p.858-876.
5. Cortie DL, Causer GL, Rule KC, Fritzsche H, Kreuzpaintner W, Klose F. Two-dimensional magnets: forgotten history and recent progress towards spintronic applications. *Advanced Functional Materials*. 2020;30(18): 1901414.
6. Niss M. History of the Lenz–Ising Model 1950–1965: from irrelevance to relevance. *Archive for History of Exact Sciences*. 2009;63(3): 243-287.
7. Wolf WP. The Ising model and real magnetic materials. *Brazilian Journal of Physics*. 2000;30(4): 794-810.

8. Lee JU, Lee S, Ryoo JH, Kang S, Kim TY, Kim P, Cheong H. Ising-type magnetic ordering in atomically thin FePS3. *Nano Letters*. 2016;16(12): 7433-7438.

9. Du KZ, Wang XZ, Liu Y, Hu P, Utama MIB, Gan CK, Kloc C. Weak van der Waals stacking, wide-range band gap, and Raman study on ultrathin layers of metal phosphorus trichalcogenides. *ACS Nano*. 2016;10(2): 1738-1743.

10. Wang X, Du K, Liu YYF, Hu P, Zhang J, Zhang Q, Xiong Q. Raman spectroscopy of atomically thin two-dimensional magnetic iron phosphorus trisulfide (FePS3) crystals. *2D Materials*. 2016;3(3): 031009.

11. Lee S, Choi KY, Lee S, Park BH, Park JG. Tunneling transport of mono-and few-layers magnetic van der Waals MnPS3. *APL Materials*. 2016;4(8): 086108.

12. Lin MW, Zhuang HL, Yan J, Ward TZ, Puretzky AA, Rouleau CM, Xiao K. Ultrathin nanosheets of CrSiTe 3: a semiconducting two-dimensional ferromagnetic material. *Journal of Materials Chemistry C*. 2016;4(2): 315-322.

13. Huang B, Clark G, Navarro-Moratalla E, Klein DR, Cheng R, Seyler KL, Xu X. Layer-dependent ferromagnetism in a van der Waals crystal down to the monolayer limit. *Nature*. 2017;546(7657): 270-273.

14. Casto LD, Clune AJ, Yokosuk MO, Musfeldt JL, Williams TJ, Zhuang HL, Mandrus D. Strong spin-lattice coupling in CrSiTe3. *APL Materials*. 2015;3(4): 041515.

15. Williams TJ, Aczel AA, Lumsden MD, Nagler SE, Stone MB, Yan JQ, Mandrus D. Magnetic correlations in the quasi-two-dimensional semiconducting ferromagnet CrSiTe 3. *Physical Review B*. 2015;92(14): 144404.

16. Carteaux V, Brunet D, Ouvrard G, Andre G. Crystallographic, magnetic and electronic structures of a new layered ferromagnetic compound Cr2Ge2Te6. *Journal of Physics: Condensed Matter*. 1995;7(1): 69.

17. Ji H, Stokes RA, Alegria LD, Blomberg EC, Tanatar MA, Reijnders A, Cava RJ. A ferromagnetic insulating substrate for the epitaxial growth of topological insulators. *Journal of Applied Physics*. 2013;114(11): 114907.

18. Alegria LD, Ji H, Yao N, Clarke JJ, Cava RJ, Petta JR. Large anomalous Hall effect in ferromagnetic insulator-topological insulator heterostructures. *Applied Physics Letters*. 2014;105(5): 053512.

19. Zhang X, Zhao Y, Song Q, Jia S, Shi J, Han W. Magnetic anisotropy of the single-crystalline ferromagnetic insulator Cr2Ge2Te6. *Japanese Journal of Applied Physics*. 2016;55(3): 033001.

20. Yang D, Yao W, Chen Q, Peng K, Jiang P, Lu X, Zhou X. Cr2Ge2Te6: high thermoelectric performance from layered structure with high symmetry. *Chemistry of Materials*. 2016;28(6): 1611-1615.

21. Liu S, Yuan X, Zou Y, Sheng Y, Huang C, Zhang E, Xiu F. Wafer-scale two-dimensional ferromagnetic Fe3GeTe2 thin films grown by molecular beam epitaxy. *2D Materials and Applications*. 2017;(1): 1-7.

22. Pei QL, Luo X, Lin GT, Song JY, Hu L, Zou YM, Sun YP. Spin dynamics, electronic, and thermal transport properties of two-dimensional CrPS4 single crystal. *Journal of Applied Physic*. 2016;119(4): 043902.

23. Mayorga-Martinez CC, Sofer Z, Sedmidubsky D, Huber S, Eng AYS, Pumera M. Layered metal thiophosphite materials: magnetic, electrochemical, and electronic properties. *ACS Applied Materials & Interfaces*. 2017;9(14): 12563-12573.

24. McGuire MA, Garlea VO, Santosh KC, Cooper VR, Yan J, Cao H, Sales BC. Antiferromagnetism in the van der Waals layered spin-lozenge semiconductor CrTe3. *Physical Review B*. 2017;95(14): 144421.

25. McGuire MA, Clark G, Santosh KC, Chance WM, Jellison Jr GE, Cooper VR, Sales BC. Magnetic behavior and spin-lattice coupling in cleavable van der Waals layered CrCl 3 crystals. *Physical Review Materials*. 2017;1(1): 014001.

26. Sun X, Yao T, Hu Z, Guo Y, Liu Q, Wei S, Wu C. In situ unravelling structural modulation across the charge-density-wave transition in vanadium disulfide. *Physical Chemistry Chemical Physics*. 2015;17(20): 13333-13339.

27. Zhong D, Seyler KL, Linpeng X, Cheng R, Sivadas N, Huang B, Xu X. Van der Waals engineering of ferromagnetic semiconductor heterostructures for spin and valleytronics. *Science Advances*. 2017;3(5): e1603113.

28. Yang J, Wang W, Liu Y, Du H, Ning W, Zheng G, Zhang Y. Thickness dependence of the charge-density-wave transition temperature in VSe2. *Applied Physics Letters*. 2014;105(6): 063109.

29. Shao Y, Song S, Wu X, Qi J, Lu H, Liu C, Gao HJ. Epitaxial fabrication of two-dimensional NiSe2 on Ni (111) substrate. *Applied Physics Letters*. 2017;111(11): 113107.

30. Huang B, Clark G, Navarro-Moratalla E, Klein DR, Cheng R, Seyler KL, Xu X. Layer-dependent ferromagnetism in a van der Waals crystal down to the monolayer limit. *Nature*. 2017;546(7657): 270-273.

31. Kuo CT, Neumann M, Balamurugan K, Park HJ, Kang S, Shiu HW, Park JG. Exfoliation and Raman spectroscopic fingerprint of few-layer NiPS3 van der Waals crystals. *Scientific Reports*. 2016;6(1): 1-10.

32. Kuo CT, Balamurugan K, Shiu HW, Park HJ, Sinn S, Neumann M, Noh TW. The energy band alignment at the interface between mechanically exfoliated few-layer NiPS3 nanosheets and ZnO. *Current Applied Physics*. 2016;16(3): 404-408.

33. Xing W, Chen Y, Odenthal PM, Zhang X, Yuan W, Su T, Han W. Electric field effect in multilayer Cr2Ge2Te6: a ferromagnetic 2D material. *2D Materials*. 2017;4(2): 024009.

34. Chu J, Wang F, Yin L, Lei L, Yan C, Wang F, He J. High-performance ultraviolet photodetector based on a few-layered 2D NiPS3 nanosheet. *Advanced Functional Materials*. 2017;27(32): 1701342.

35. Kresse Georg. VASP the Guide. Available from: http://cms. mpi. univie. ac. at/vasp.

36. Hazen RM, Downs RT, Prewitt CT. Principles of comparative crystal chemistry. *Reviews in Mineralogy and Geochemistry*. 2000;41(1): 1-33.

37. Tang W, Sanville E, Henkelman G. A grid-based Bader analysis algorithm without lattice bias. *Journal of Physics: Condensed Matter*. 2009;21(8): 08420

38. Wood DL, Ferguson J, Knox K, Dillon Jr JF. Crystal-field spectra of d 3, 7 ions. III. Spectrum of Cr3+ in various octahedral crystal fields. *Journal of Chemical Physics*. 1963;39(4): 890-898.

39. Naruse Y, Takamori A. Orbital Phase Perspective of Goodenough-Kanamori-Anderson Rules (GKA Rules) in Superexchange Interaction. 2020. ChemRxiv [Preprint]. Available from: 10.26434/chemrxiv.10251563.v2.

# THE AUTHORS

**Maria S. Baranava**
e-mail: baranova@bsuir.by
ORCID: 0000-0002-2618-4464

**Viktor R. Stempitsky**
e-mail: vstem@bsuir.by
ORCID: 0000-0001-9362-7539